Active Noise Control of Vibroacoustic Noise from HVAC System in Autonomous Bus Using Conjugate Gradient-based Algorithm

Orhun Okcu, Seongyeol Kim
AVSP Laboratory, Inha University, Incheon, South Korea
{orhun.okcu,seongyeolk}@inha.edu

Sangkwon Lee
AVSP Laboratory, Inha University, Incheon, South Korea
sangkwon@inha.ac.kr

Abstract

In future autonomous buses, heating, ventilation, and air-conditioning (HVAC) system is installed under each passenger's seat to provide air conditioning for each passenger. Therefore, the sound radiated from the compressor of the HVAC system is a very high-frequency annoyance noise caused by vibroacoustic noise due to the shell vibration of the compressor. The HVAC system generates vibroacoustic noise dominantly in the frequency range between 200 and 600 Hz. The dominant frequency components of that noise are harmonics of the rotation frequency of the reciprocating compressor. Such noise is not only distinctly perceptible but also contributes to passenger discomfort and negatively impacts the perceived quality of the vehicle. The aim of this paper is to attenuate the vibroacoustic noise of the HVAC system by developing an active noise control (ANC) system. Generally, the widely recognized filtered-X least mean squared (FXLMS) algorithm has been successfully implemented to active noise control of reciprocating compressor. However, its performance was found lacking outside the peak frequency of compressor operation noise. To address this, the conjugate gradient algorithm was employed to enhance ANC performance. The conjugate gradient algorithm has a lower residual error and faster convergence rate compared to the FXLMS algorithm. As a result of this, the noise reduction where outside of the peak frequency of compressor operation noise was increased thanks to the conjugate gradient-based ANC algorithm.

Keywords: HVAC noise; Active Noise Control; Conjugate gradient algorithm; and LMS algorithm

1 Introduction

The acoustic emissions from the HVAC have recently emerged as significant contributors to the overall noise within electric vehicle cabins. This HVAC noise profoundly affects passenger riding comfort. Consequently, extensive research efforts have been devoted to analyzing and reducing these noises. Research has shown that elements like the air flow rate and the kind of engine, whether it's an internal combustion engine (ICEV) or a hybrid (HEV), are crucial in assessing aspects like annoyance, loudness, and the degree of pleasantness. Furthermore, an increase in the airflow rate is associated with a reduction in the perceived level of pleasantness [1]. On the other hand, sound quality indices can be used to design an HVAC noise. The desired spectrum is shaped to achieve a high pleasant and cool index using subjective evaluation of noise [2]. Contrasting with typical vehicle HVAC systems, the HVAC system in autonomous bus seats is structurally akin to refrigerator systems, incorporating components like compressors, evaporators, condensers, and fans. This similarity allows for the application of noise control techniques used in refrigerator systems to be effectively employed in autonomous car seat HVAC systems. Among these HVAC parts, the shell vibration of the compressor generates noise that is harmonic to the rotation frequency of the reciprocating compressor.

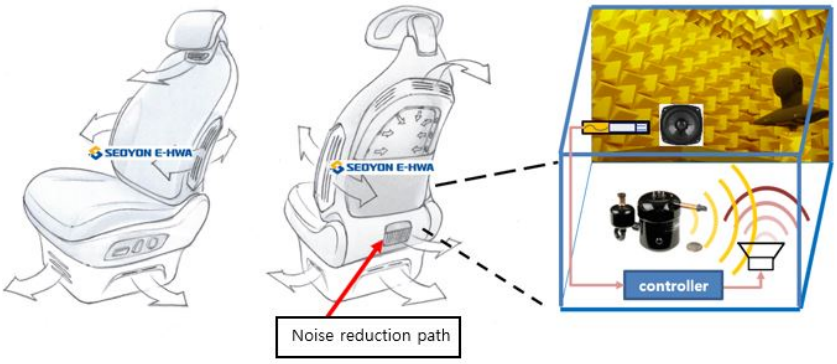

Figure 1: The HVAC system of the autonomous bus seat

The hybrid technique, a combination of passive and active techniques, can be used to obtain a reduction in the overall frequency range for this dominant noise. ANC stands out as a technique for suppressing low-frequency noise, offering the advantage of effective noise reduction without additional weight or space consumption, and without impeding airflow, unlike many passive methods [3]. On the other hand, passive strategies such as sound-absorbing materials are more suited for high-frequency noise reduction [4]. For

example, the vibration absorber can be designed to reduce such structural vibration in the high-frequency range [5]. ANC operates by producing 'anti-noise' of equal amplitude but opposite phase to the primary noise. Adaptive filtering, often employing the LMS algorithm, is a cornerstone of ANC systems for addressing time-varying noise characteristics [6]. Despite its effectiveness, there are space constraints within the system that limit the speaker size, affecting low-frequency noise reduction. Therefore, the low-frequency component of the output can be filtered out [7]. Moreover, the projection onto convex sets (POCS) technique has been implemented to increase the performance of the ANC system [8]. In this study, on the other hand, a frequency range between 200 Hz and 600 Hz is targeted for this ANC application since the speaker to be used has a diameter of 2.25 inches. However, this frequency range is relatively high for the ANC application because the generation of a signal that is out of phase of the high-frequency primary noise signal is challenging due to its short wavelength. Hence, the ANC algorithm requires fast convergence. For the ANC algorithm, the FXLMS algorithm is widely used because it is robust and requires low computation. However, the convergence speed of the LMS algorithm is poor due to a phenomenon called eigenvalue spread [9]. The performance of the LMS algorithm can be improved using the Conjugate-gradient algorithm with a small increase in computational burden [10]. The algorithm updates the search direction that conjugate with the autocorrelation matrix. Therefore, the conjugate gradient-based algorithm offers faster convergence and reduced residual error compared to the LMS algorithm. This algorithm is successfully implemented and analyzed in the context of adaptive filtering theory [11]. In addition, there is only one study that theoretically implements this algorithm in the ANC system [12]. In this study, the Conjugate gradient-based ANC algorithm will be developed for the HVAC system for autonomous bus seats. The study includes measuring sound intensity and pressure levels. These measurements guide the placement of error microphones. Subsequently, a coherence analysis is conducted between these microphones and the compressor shell's vibration, serving as the reference signal, to select the optimal reference for the ANC technique. Initially, the FXLMS algorithm was applied for noise control. However, its performance was found lacking outside the peak frequency of compressor operation noise. To address this, the conjugate gradient algorithm was employed to enhance ANC performance. Finally, the study compares the noise reduction and convergence efficiency of both algorithms, highlighting the improved outcomes achieved with the conjugate gradient approach.

2 Theory of the Least Mean Square (LMS) Algorithm

The fundamental objective of the Least Mean Square (LMS) algorithm is to ascertain the optimal filter coefficients that minimize the mean square error. This optimization employs the iterative steepest descent method, where each iteration proceeds in the direction opposite to the gradient of the error surface [6].

$$\mathbf{w}(n+1) = \mathbf{w}(n) + \mu(-\nabla_n) \tag{1}$$

The error signal, $e(n)$, is defined as the difference between the desired signal, $d(n)$, and the output signal, $y(n) = x(n)\mathbf{W}(n)$.

$$e(n) = d(n) - x(n)\mathbf{w}(n) \tag{2}$$

Accordingly, the gradient of the squared error is expressed as

$$\nabla e^2(n) = -2e(n)x(n) \tag{3}$$

Substituting Equation 3 into Equation 1, the final form of the LMS algorithm is obtained.

$$\mathbf{w}(n+1) = \mathbf{w}(n) + \mu e(n)x(n) \tag{4}$$

Here, μ denotes the convergence factor, crucial for the stability and steady-state effectiveness of the algorithm. The algorithm employs a time-varying step size, calculated to be inversely proportional to both the power of the reference signal ($\hat{P}_x$) and the filter's length L. This is expressed as

$$\mu(n) = \frac{\alpha}{L\hat{P}_x(n)} \tag{5}$$

Here, the normalized step size α falls within the range of $0 < \alpha < 2$. The power of the reference signal is estimated using the formula

$$\hat{P}_x(n) = \frac{1}{M}\sum_{m=0}^{M-1} x^2(n-m). \tag{6}$$

To mitigate divergence issues due to insufficient spectral excitation, a leaky mechanism is integrated into the weight update process. The leaky LMS algorithm is thus formulated as follows

$$\mathbf{w}(n+1) = \nu\mathbf{w}(n) + \mu x(n)e(n) \tag{7}$$

In this context, ν denotes the leakage factor, constrained within the range $0 < \nu \leqslant 1$. Adjusting the leakage factor involves a trade-off between robustness and performance loss [3]. In practical implementations involving electronic components such as microphones, filters, and amplifiers, the signal path from the loudspeaker to the error microphone, termed the secondary path, significantly influences the ANC system's efficacy. Burgess [13] proposed compensating for the secondary path effect to enhance system performance. This is achieved by filtering the reference signal with a filter that mimics the secondary path, leading to the development of the Filtered-X LMS (FXLMS) algorithm. The error signal in the FXLMS context is redefined as follows

$$\hat{x}(n) = s(n) * x(n) \tag{8}$$

where $s(n)$ is the impulse response of secondary path, $*$ denotes linear convolution. The gradient of squared error can be rewritten as

$$\nabla e(n) = -2\hat{x}(n)e(n). \tag{9}$$

The FXLMS algorithm iteratively updates the filter weights to achieve optimum noise cancellation

$$\mathbf{w}(n+1) = \nu\mathbf{w}(n) + \mu\hat{x}(n)e(n) \tag{10}$$

Since the transfer function $S(z)$ of the secondary path is typically unknown, it can be estimated via a separate LMS algorithm. The adaptive filter output is computed by linear convolution between the optimum filter and the reference signal.

$$y(n) = \sum_{l=0}^{L} w_l(n)\hat{x}(n-l) \tag{11}$$

The block diagram of the FXLMS algorithm is shown in Figure 2.

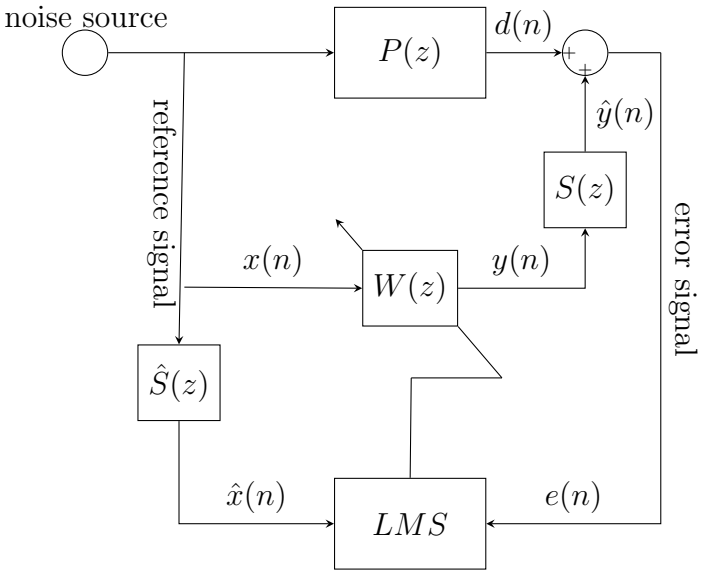

Figure 2: Block diagram of ANC system using the FXLMS Algorithm

In this representation, $\hat{S}(z)$ denotes the estimated transfer function of the secondary path, $P(z)$ represents the primary path, and $W(z)$ symbolizes the time-varying adaptive filter.

3 Conjugate Gradient Algorithm

Conjugate direction methods strike a balance between the steepest descent approach and Newton's method. They aim to enhance the efficiency often lacking in the steepest descent, without needing the extensive data handling, like evaluation and manipulation of the Hessian matrix, that Newton's method requires. However, the conjugate gradient algorithm does not require the computation of the inverse of the Hessian matrix ($\mathbf{R}^{-1}$). Conjugate direction methodologies, with an emphasis on the conjugate gradient technique, have established their proficiency in efficiently addressing not only the quadratic cost function but also the general objective functions [14]. The conjugate gradient algorithm has comparable performance to the RLS algorithm which is more computationally intensive than the conjugate gradient algorithm [11]. On the other hand, the LMS algorithm is sensitive to step size μ and has slow convergence due to the eigenvalue spread which is related to the autocorrelation matrix of the input signal [9]. The cost function to be minimized is the same as the LMS algorithm which is the square of the error signal.

$$F(\mathbf{w}(n)) = \frac{1}{2}\mathbf{w}(n)^T\mathbf{R}\mathbf{w}(n) - \mathbf{p}^T\mathbf{w}(n) + \frac{1}{2}E[d^2(n)] \tag{12}$$

where $\mathbf{R}$ is the autocorrelation matrix of input matrix

$$\begin{aligned}\mathbf{R} &\equiv E[\mathbf{x}(n)\mathbf{x}^T(n)] \\ &= \begin{bmatrix} r_{xx}(0) & r_{xx}(1) & \cdots & r_{xx}(L-1) \\ r_{xx}(1) & r_{xx}(0) & \cdots & r_{xx}(L-2) \\ \vdots & \cdots & \ddots & \vdots \\ r_{xx}(L-1) & r_{xx}(L-2) & \cdots & r_{xx}(0) \end{bmatrix}\end{aligned} \tag{13}$$

where

$$r_{xx}(k) \equiv E[x(n)x(n-k)] \tag{14}$$

and $\mathbf{p}$ is the cross-correlation matrix between desired and input signal.

$$\begin{aligned}\mathbf{p} &\equiv E[d(n)\mathbf{x}(n)] \\ &= \begin{bmatrix} r_{dx}(0) & r_{dx}(1) & \cdots & r_{dx}(L-1) \end{bmatrix}^T\end{aligned} \tag{15}$$

where

$$r_{dx}(k) \equiv E[d(n)x(n-k)] \tag{16}$$

The optimal filter coefficient can be computed by taking the partial derivative with respect to the filter and equating to zero. Consequently, it becomes,

$$\mathbf{R}\mathbf{w}^{\circ}(n) = \mathbf{p} \tag{17}$$

where $\mathbf{w}^{\circ}(n)$ is the optimum filter. Therefore, the gradient which is the negative of the residual $\mathbf{r}(n)$ is

$$\begin{aligned}\mathbf{g}(n) &= -\mathbf{r}(n) = \mathbf{R}(n)\mathbf{w}(n) - \mathbf{p} \\ &= [\mathbf{w}(n)\mathbf{x}(n) - d(n)]\mathbf{x}(n) \\ &= -e(n)\mathbf{x}(n)\end{aligned} \tag{18}$$

The algorithm error can defined as

$$\boldsymbol{\varepsilon}(n) = \mathbf{w}(n) - \mathbf{w}^{\circ}(n) \tag{19}$$

We can rewrite the residual in terms of the algorithm error

$$\begin{aligned}\mathbf{r}(n) &= \mathbf{p} - \mathbf{R}(n)\mathbf{w}(n) \\ &= \mathbf{R}(\mathbf{w}^{\circ}(n) - \mathbf{w}(n)) \\ &= -\mathbf{R}\boldsymbol{\varepsilon}(n)\end{aligned} \tag{20}$$

While the LMS algorithm utilizes residual as a search direction and search directions are orthogonal to each other. The search direction of the conjugate gradient algorithm is conjugate with $\mathbf{R}$ (R-orthogonality) which is the second derivative of the cost function (Hessian matrix) [15].

$$\mathbf{d}(i)^T\mathbf{R}\mathbf{d}(j) = 0, \quad \text{for all} \quad i \neq j \tag{21}$$

The filter coefficient can be updated using this search direction.

$$\mathbf{w}(n+1) = \mathbf{w}(n) + \alpha\mathbf{d}(n) \tag{22}$$

Taking the derivative with respect to α and equating to zero of Equation 12 gives R-orthogonality.

$$\begin{aligned} \frac{d}{d\alpha}F(\mathbf{w}(n+1)) &= 0 \\ F'(\mathbf{w}(n+1))^T\frac{d}{d\alpha}\mathbf{w}(n+1) &= 0 \\ -\mathbf{r}^T(n+1)\mathbf{d}(n) &= 0 \\ \mathbf{d}^T(n)\mathbf{R}\boldsymbol{\varepsilon}(n+1) &= 0 \end{aligned} \tag{23}$$

In other words, the next step can be thought of as an algorithm error which is conjugated with $\mathbf{R}$ [16]. The search direction can be constructed by the residual and previous search directions.

$$\mathbf{d}(n) = \mathbf{r}(n) + \sum_{k=0}^{n-1}\beta_{nk}\mathbf{d}(k) \tag{24}$$

where β_{nk} are defined for $i > k$. To compute the β_{nk}, the Equation 24 can be multiplied by $\mathbf{d}^T(m)\mathbf{R}$. Thus, it becomes

$$\begin{aligned} \mathbf{d}^T(n)\mathbf{R}\mathbf{d}(m) &= \mathbf{r}^T(n)\mathbf{R}\mathbf{d}(m) + \sum_{k=0}^{n-1}\beta_{nk}\mathbf{d}^T(k)\mathbf{R}\mathbf{d}(m) \\ 0 &= \mathbf{r}^T(n)\mathbf{R}\mathbf{d}(m) + \beta_{nk}\mathbf{d}^T(m,)\mathbf{R}\mathbf{d}(m), \quad n > m \quad \text{(by } \mathbf{R} \text{ -orthogonality)} \\ \beta_{nk} &= -\frac{\mathbf{r}^T(n)\mathbf{R}\mathbf{d}(m)}{\mathbf{d}^T(m)\mathbf{R}\mathbf{d}(m)}. \end{aligned} \tag{25}$$

The residual can be computed iteratively using Equation 20.

$$\begin{aligned} \mathbf{r}(n+1) &= -\mathbf{R}\boldsymbol{\varepsilon}(n+1) \\ &= -\mathbf{R}(\boldsymbol{\varepsilon}(n) + \alpha(n)\mathbf{d}(n)) \\ &= \mathbf{r}(n) - \alpha(n)\mathbf{R}\mathbf{d}(n) \end{aligned} \tag{26}$$

Multiplication of the recursive residual equation above with $\mathbf{r}(k)$ gives

$$\begin{aligned} \mathbf{r}^T(k)\mathbf{r}(n+1) &= \mathbf{r}^T(k)\mathbf{r}(n) - \alpha(n)\mathbf{r}^T(k)\mathbf{R}\mathbf{d}(n) \\ \alpha(n)\mathbf{r}^T(k)\mathbf{R}\mathbf{d}(n) &= \mathbf{r}^T(k)\mathbf{r}(n) - \mathbf{r}^T(k)\mathbf{r}(n+1) \end{aligned} \tag{27}$$

From the equation above we can compute the numerator of the Equation 25.

$$\mathbf{r}^T(k)\mathbf{R}\mathbf{d}(n) = \begin{cases} \frac{1}{\alpha(k)}\mathbf{r}^T(k)\mathbf{r}(k), & k = n, \\ -\frac{1}{\alpha(k-1)}\mathbf{r}^T(k)\mathbf{r}(k), & k = n+1, \\ 0, & \text{otherwise.} \end{cases} \tag{28}$$

Substituting the equation above into the Equation 25 gives

$$\beta_{nk} = \begin{cases} \frac{1}{\alpha(k-1)} \frac{\mathbf{r}^T(k)\mathbf{r}(k)}{\mathbf{d}^T(k-1)\mathbf{R}\mathbf{d}(k-1)}, & k = n+1 \\ 0, & k > n+1 \end{cases} \tag{29}$$

The step size $\alpha(k)$ can be derived using the Equation 23.

$$\begin{aligned} \mathbf{d}^T(n)\mathbf{R}\boldsymbol{\varepsilon}(n+1) &= 0 \\ \mathbf{d}^T(n)\mathbf{R}(\boldsymbol{\varepsilon}(n) + \alpha(n)\mathbf{d}(n)) &= 0 \\ \alpha(n) &= -\frac{\mathbf{d}^T(n)\mathbf{R}\boldsymbol{\varepsilon}(n)}{\mathbf{d}^T(n)\alpha(n)\mathbf{d}(n)} \\ \alpha(n) &= -\frac{\mathbf{d}^T(n)\mathbf{r}(n)}{\mathbf{d}^T(n)\mathbf{R}\mathbf{d}(n)} \end{aligned} \tag{30}$$

Substitution of the step size into the Equation 29 gives

$$\beta(n) = \frac{\mathbf{r}^T(n)\mathbf{r}(n)}{\mathbf{d}^T(n-1)\mathbf{r}(n-1)} \tag{31}$$

On the other hand, residual at any point is orthogonal to the ellipsoidal error surface at any point. It can be proved using the expanding subspace theorem [14]. To show this mathematically, the algorithm error can be written as a linear combination of search direction $\mathbf{d}(n)$.

$$\boldsymbol{\varepsilon}(j) = \sum_{j=i}^{n-1} \delta(j)\mathbf{d}(j) \tag{32}$$

This equation can be multiplied by $-\mathbf{d}^T(i)\mathbf{R}$ to eliminate the right-hand side of the equation.

$$\begin{aligned} -\mathbf{d}^T(i)\mathbf{R}\boldsymbol{\varepsilon}(j) &= -\sum_{j=i}^{n-1}\delta(j)\mathbf{d}^T(i)\mathbf{R}\mathbf{d}(j) \\ \mathbf{d}^T(i)\mathbf{r}(n) &= 0, \quad i<j \quad \text{(by } \mathbf{R}\text{ -orthogonality)} \end{aligned} \tag{33}$$

The useful identity can be derived by multiplying the Equation 24 with $\mathbf{r}(m)$

$$\begin{aligned} \mathbf{d}^T(n)\mathbf{r}(m) &= \mathbf{r}^T(n)\mathbf{r}(m) + \sum_{k=0}^{n-1}\beta_{nk}\mathbf{d}^T(k)\mathbf{r}(m) \\ \mathbf{d}^T(n)\mathbf{r}(m) &= \mathbf{r}^T(n)\mathbf{r}(m) \end{aligned} \tag{34}$$

Using this identity, the Equation 31 becomes

$$\begin{aligned} \beta(n) &= \frac{\mathbf{r}^T(n)\mathbf{r}(n)}{\mathbf{r}^T(n-1)\mathbf{r}(n-1)} \\ &= \frac{\mathbf{g}(n)^T\mathbf{g}(n)}{\mathbf{g}(n-1)^T\mathbf{g}(n-1)} \end{aligned} \tag{35}$$

The step size α is taken as constant to reduce computational burden which means the line search for the optimal alpha is not conducted. The final algorithm is summarized as follows.

Algorithm 1 Conjugate Gradient Algorithm

$\mathbf{W}_0 = 0$
for $i = 1, 2, 3, \cdots$ **do**
    if $i = 1$ **then**
        $\mathbf{d}(i) = -\mathbf{g}(i)$
    else
        $\beta(i) = \frac{\mathbf{g}(i+1)^T\mathbf{g}(i+1)}{\mathbf{g}(i)^T\mathbf{g}(i)}$
        $\mathbf{d}(i+1) = -\mathbf{g}(i) + \beta(i)\mathbf{d}(i)$
    end if
    $\mathbf{w}(i+1) = \mathbf{w}(i) + \alpha\mathbf{d}(i)$
end for

4 ANC of Vibroacoustic Noise from HVAC System

4.1 Flow Chart of Algorithm

The Active Noise Control (ANC) system employed in this study is characterized as a single reference with a multiple output configuration (1x2x2), as delineated in Figure 3. The system acquires a reference signal through an accelerometer stuck to the compressor's shell. Within the HVAC system, there are four speakers; however, only the speakers positioned at the front and right are utilized. This selection is based on measurements of Sound Pressure Level (SPL) and acoustic intensity. The error signals are captured by microphones strategically placed in the near field of the front and right sides of the HVAC system. These reference and error signals are crucial in the computation of optimal filter coefficients, a process executed utilizing Equations 10 and 22. It should be noted that the reference signal undergoes a filtration process before its integration into the algorithm, facilitated by modeled secondary filters. These filters represent transfer functions that cover the characteristics of various electronic components, such as analog filters and amplifiers, as well as the acoustic pathway extending from the speakers to the error microphones. Subsequently, the derived optimal filter coefficients are convolved with the reference signal in accordance with Equation 11. This process yields the output signal $y(n)$, which functions as the anti-noise of the targeted noise signal $d(n)$.

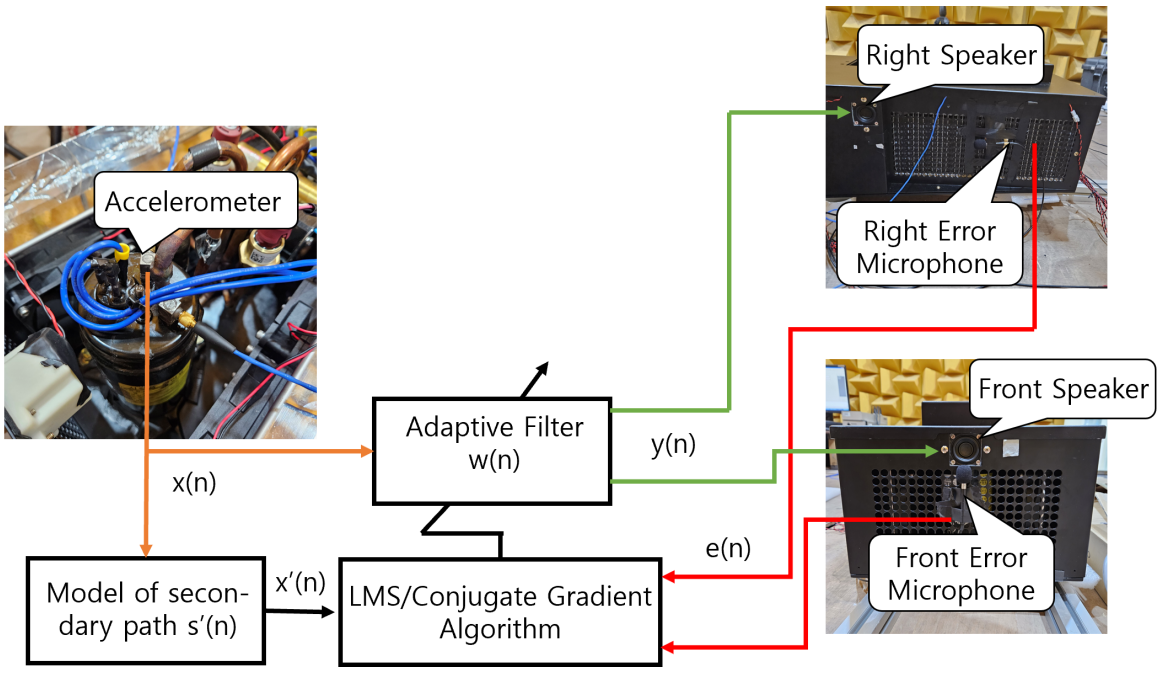

Figure 3: Configuration of the HVAC ANC system

4.2 Experimental Setup of the HVAC ANC System

The experimental setup entailed the utilization of a notebook computer interfaced with the dSPACE Autobox I/O board as shown in Figure 4. The dSPACE Autobox plays a crucial role in this setup, facilitating the conversion of signals from analog to digital and vice versa. Additionally, it executes the embedded MATLAB Simulink code designated for Active Noise Control (ANC).

The signals collected from the error microphones and the accelerometer cannot be employed in their raw form due to the indeterminate frequency content. Consequently, it becomes essential to subject these signals to a low-pass filtering process. This step aids in determining the appropriate sampling frequency. The low-pass filters are configured with a cut-off frequency of 700 Hz, marginally exceeding the highest frequency target for ANC.

To prevent the occurrence of aliasing, the sampling frequency must be at least twice the frequency content of the signal. In this instance, a sampling frequency of 2048 Hz is selected, exceeding the double threshold of the signal's frequency content. Moreover, the output signal $y(n)$, directed towards the speakers, requires filtering to correct any reconstruction errors that may arise during the digital-to-analog conversion process. The cut-off frequency for this reconstruction filter is also set at 700 Hz. Finally, this signal is amplified using an amplifier to effectively drive the loudspeakers.

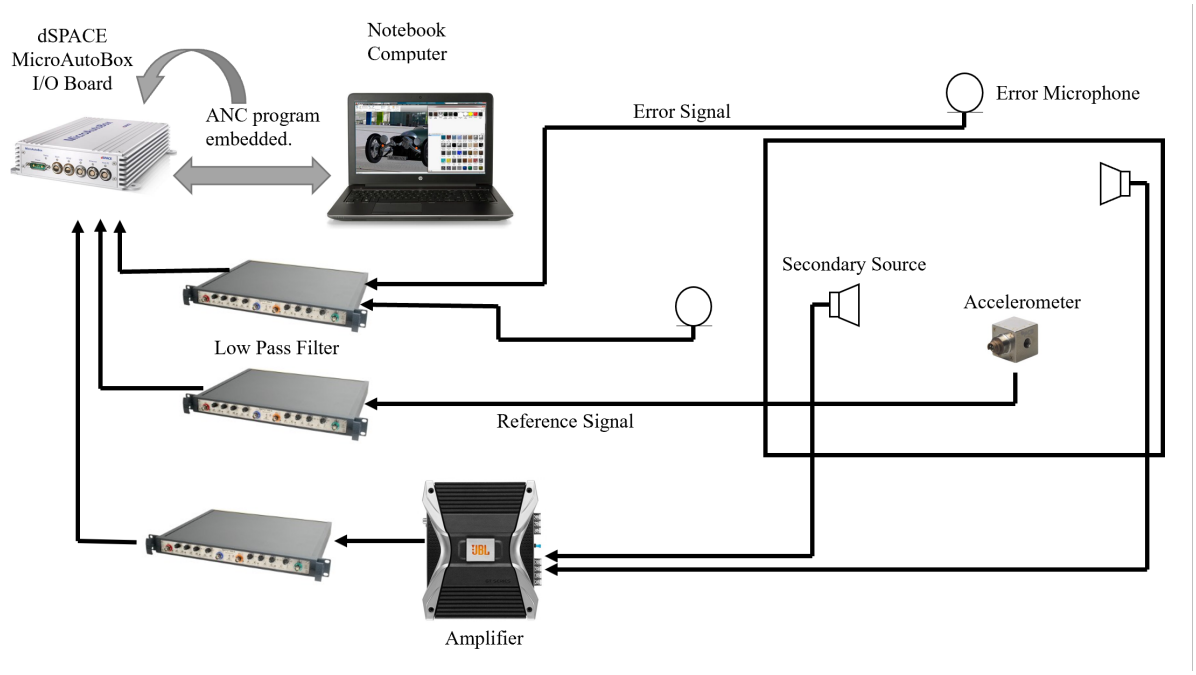

Figure 4: Experimental setup for implementation of ANC system

4.3 Placement of the Error Microphone

The microphones have been replaced within a 1-meter distance in accordance with the stipulated standards. The measurement setup is depicted in Figure 5.

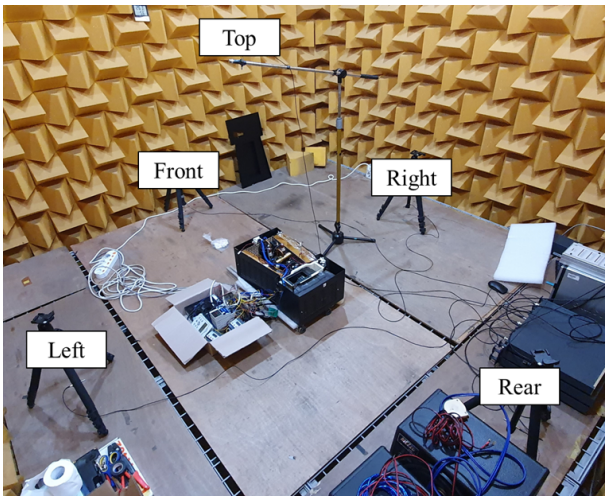

Figure 5: SPL measurement setup for the HVAC system

The A-weighted sound pressure level (SPL) in the overall frequency range (0-5000 Hz) is presented in Table 1.

Table 1: A-weighted sound pressure level of all microphones

Microphones	**Front**	**Right**	**Left**	**Rear**	**Top**
Average SPL	60.30 dB	60.14 dB	56.62 dB	57.26 dB	56.10 dB

It is noteworthy that the data acquired from the front and right microphones have been selected to serve as the error signal $e(n)$ in the algorithm. This decision is based on the observation that these microphones exhibit the highest SPL values. Intensity can be described as the quantity of sound energy passing through a unit area perpendicular to the direction of propagation [17]. It is mathematically expressed as

$$I = \langle pu \rangle_T = \frac{1}{T} \int_0^T pu \, dt \tag{36}$$

where p is acoustic pressure, u is particle speed, and T is the period of the time. Intensity measurements are crucial for pinpointing the location of a noise source and determining the amount of sound energy [18]. The measurement of sound intensity in this context was conducted using an acoustic sensor developed by Microflown. This sensor computes particle velocity based on the temperature variances of heated platinum wires within the

probe [19]. The outcomes of these sound intensity measurements are depicted in Figure 6. The microphones have been strategically positioned at locations where the intensity of sound is comparatively higher than at other points.

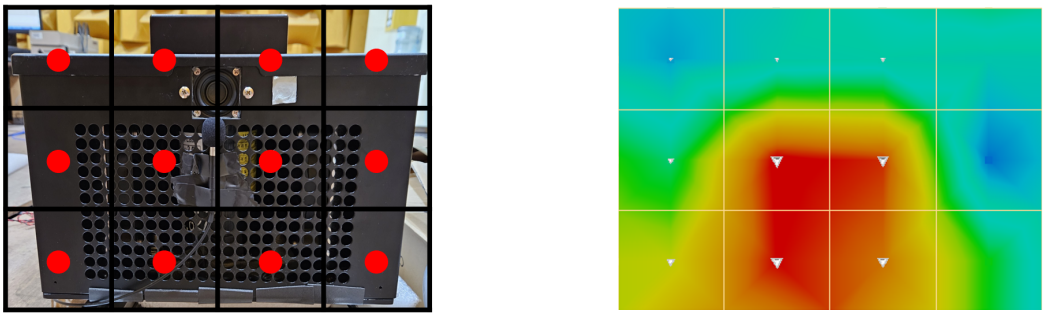

(a) Intensity measurement of the front surface of the HVAC system

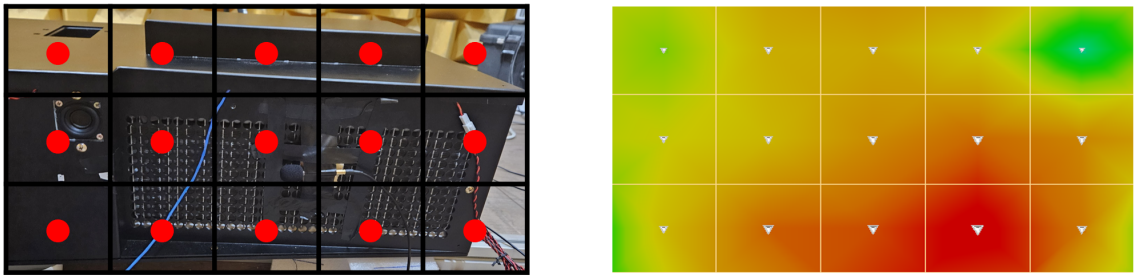

(b) Intensity measurement of the right surface of the HVAC system

Figure 6: Intensity measurement result of the HVAC System

4.4 Selection of the Reference Signal

The accelerometer data specifically collected in the z-axis direction has been employed as the reference signal $x(n)$ as shown in Figure 3. The Fourier transform of this reference signal is presented in Figure 7, offering a detailed spectral representation. The peaks in the graph denote the operation frequency of the compressor and its order.

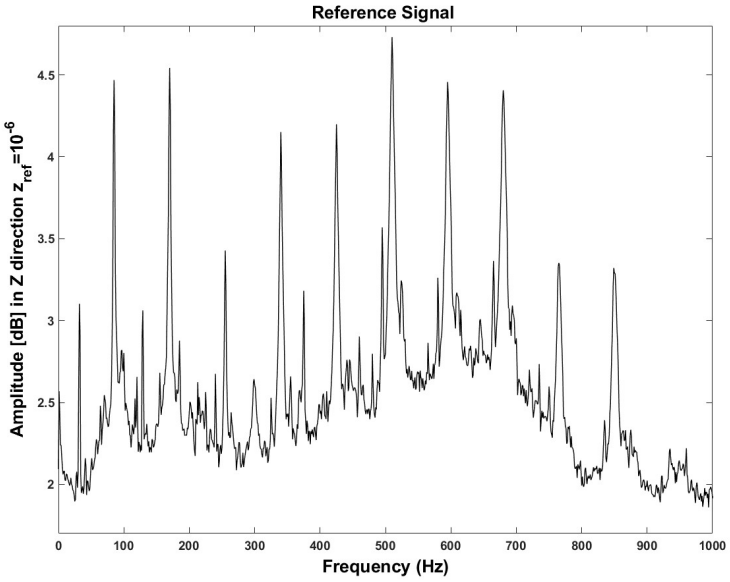

Figure 7: Fourier transform of the reference signal

The ordinary coherence function is commonly employed to assess the extent of linear association between two signals, such as input and output signals [20]. The coherence value, therefore, is an important parameter for the performance evaluation of the ANC system [3]. Thus, magnitude-squared coherence can be defined as

$$C_{dx}(f) = |\gamma_{dx}(f)|^2 = \frac{|S_{dx}(f)|^2}{S_{dd}(f)S_{xx}(f)} \tag{37}$$

where f denotes the frequency of interest, $S_{dx}(f)$ is the cross-power spectrum, and $S_{dd}(f)$ and $S_{xx}(f)$ are the autopower spectra of $d(n)$ and $x(n)$, respectively. The minimum value of the auto power spectra of the error signal can be computed as

$$S_{ee}(f) = [1 - C_{dx}(f)]S_{dd}(f). \tag{38}$$

Equation 38 indicates that to be able to apply ANC successfully, the coherence between the reference signal and noise (desired signal) must be high. The coherence values between the accelerometer signal in the z direction and front, right microphone, as depicted in Figure 8, approach unity at the operational frequency of the compressor and its harmonics. This indicates a high degree of correlation, suggesting that the vibroacoustic noise emanating from the compressor can be effectively controlled.

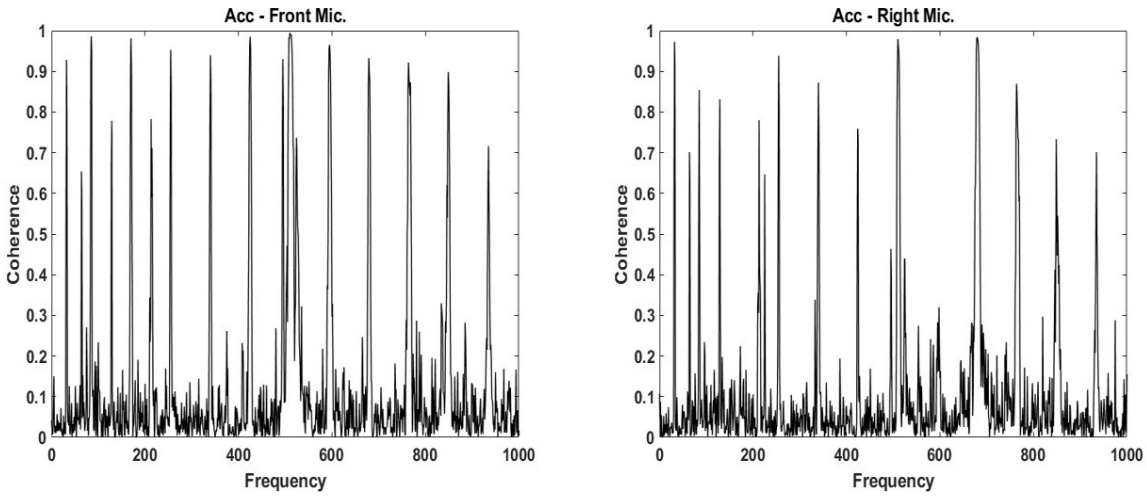

(a) Coherence value between accelerometer and front microphone signals

(b) Coherence value between accelerometer and right microphone signals

Figure 8: Coherence values between reference and desired signal

4.5 Measurement of Secondary Path

The estimation of the secondary path models, which are the transfer functions between speakers and error microphones, is based on the assumption that these models are time-invariant. Consequently, an offline modeling technique has been implemented to determine these filter coefficients. Broadband white noise, recognized as the ideal signal for such estimations due to its encompassing frequency range, is utilized in this process. This white noise is inputted into the speakers, and the consequent sound pressure is measured by the error microphones. Utilizing adaptive filter algorithms in this context facilitates the determination of the filter coefficients for the secondary paths, thereby allowing for a precise model estimation. The frequency responses of the secondary models are depicted in Figure 9.

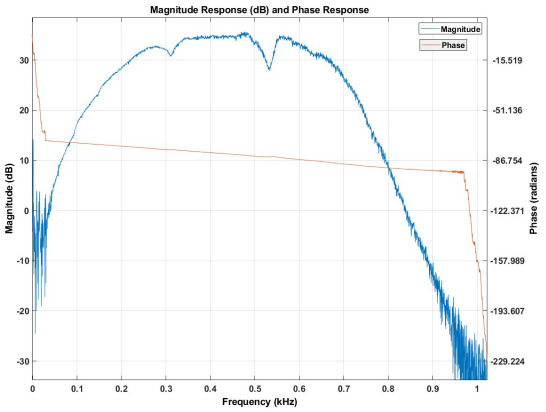

(a) Secondary path model between front speaker and front error microphone

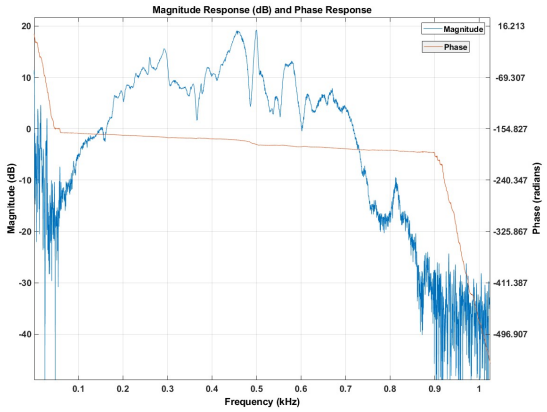

(b) Secondary path model between front speaker and right error microphone

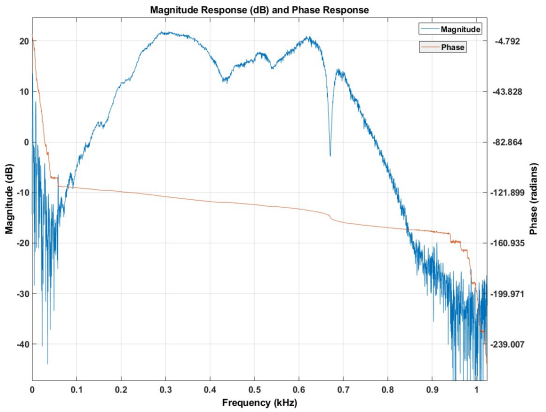

(c) Secondary path model between right speaker and front error microphone

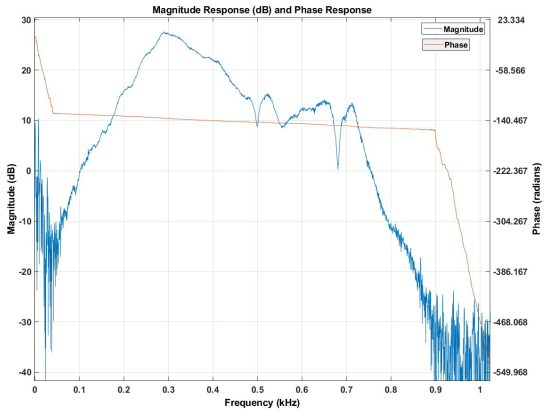

(d) Secondary path model between right speaker and right error microphone

Figure 9: Frequency responses of secondary path models

Furthermore, the estimation of the secondary path models presents an opportunity to compare the convergence performance of the two algorithms in question. This comparative analysis is illustrated in Figure 10, which showcases the convergence trajectories for each algorithm. It is observed that the mean squared error (MSE) value for the conjugate gradient algorithm converges more rapidly, accompanied by a lower magnitude of residual error. In contrast, the Least Mean Squares (LMS) algorithm demonstrates a slower rate of convergence, coupled with a less favorable performance in terms of residual error. This contrast highlights the relative efficiencies and limitations of the two algorithms within the context of model estimation.

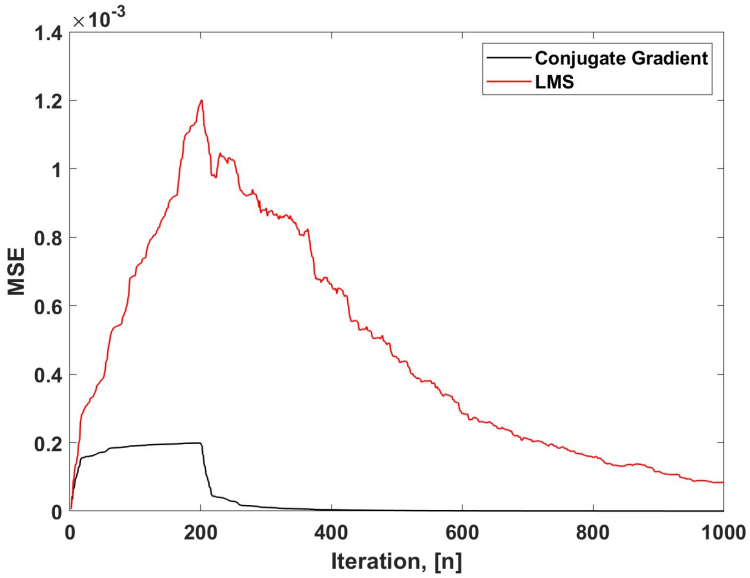

Figure 10: Comparison of the convergence performance

4.6 Results of the ANC

The discrete Fourier transforms (DFTs) of the signals captured by the error microphones are graphically represented in Figure 11. Within this figure, it is evident that the conjugate gradient algorithm exhibits superior performance compared to the FXLMS algorithm, particularly in terms of reducing the peak frequencies. This superior performance is not limited to the peak frequencies alone; it also extends to the frequency ranges outside of these peaks, as observed for the front microphone. For the right microphone, the performance of the peak reduction across the frequency spectrum is notably similar between the algorithms, except for the peak at 255 Hz. However, the conjugate gradient algorithm demonstrates enhanced effectiveness, particularly in the frequency ranges outside of these peaks.

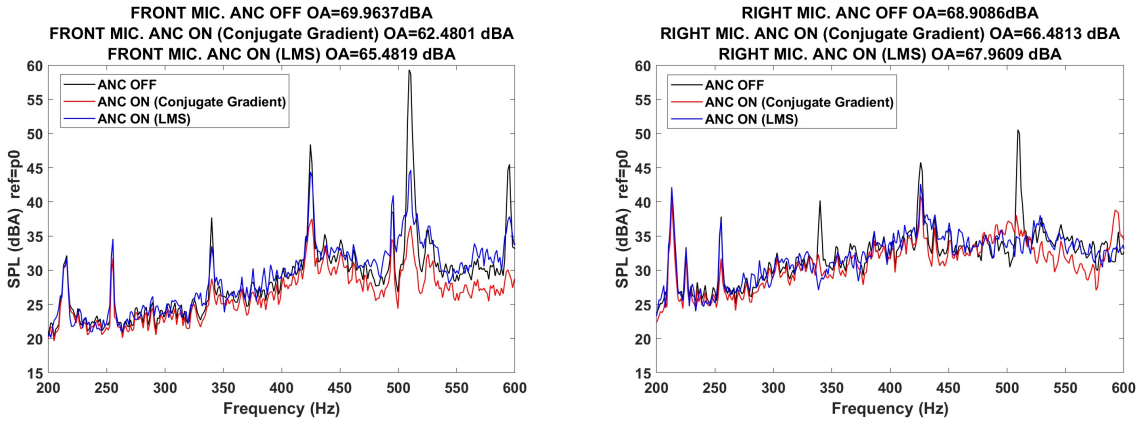

(a) Fourier transform of the front microphone (b) Fourier transform of the right microphone

Figure 11: Fourier transform of the error microphone data without and with ANC

5 Conclusion

In this study, we present the implementation of a conjugate gradient algorithm within the HVAC system of an autonomous bus seat. The HVAC system is a significant source of vibroacoustic noise, predominantly within the 200 to 600 Hz frequency range. This noise is primarily due to the vibration of the compressor's shell at the rotation frequency and its harmonics, resulting in prominent peaks in the frequency response. To control these disruptive noises, an ANC system has been developed. Initially, error microphones were strategically placed on the front and right surfaces of the HVAC system, guided by SPL and intensity measurements. The reference signal for the ANC system was derived from an accelerometer stuck to the compressor's shell. High coherence between the accelerometer data in the z-axis and the noise peaks was observed, indicating the potential efficacy of the ANC system. Following the estimation of the secondary path transfer functions, the feedforward ANC was implemented using both the traditional FXLMS algorithm and the novel conjugate gradient algorithm. The study concludes that the conjugate gradient algorithm outperforms the FXLMS algorithm in reducing the overall noise levels of the HVAC system.

References

[1] Massimiliano Masullo, Katsuya Yamauchi, Minori Dan, Federico Cioffi, and Luigi Maffei. Intercultural differences in the perception of hvac sound quality in car cabins: From conventional to electric vehicles. *Applied Sciences*, 11(23):11431, 2021.

[2] Jiseon Back, Sang-Kwon Lee, Seung Min Lee, Kanghyun An, Dong-Ho Kwon, and

Dong-Chul Park. Design and implementation of comfort-quality hvac sound inside a vehicle cabin. *Applied Acoustics*, 177:107940, 2021.

[3] Sen M Kuo and Dennis R Morgan. *Active noise control systems*, volume 4. Wiley, New York, 1996.

[4] DG Smith, MF Arnold, EW Ziegler, Kh Eghtesadi, and M Brown. A systems approach to appliance compressor quieting using active noise control techniques. 1992.

[5] Wongul Hwang, Ilkwon Oh, Byounggu Kim, Sungwoo Park, and Kio Ryu. A study on noise radiation from compressor shell. 2006.

[6] Widrow Bernard and D Stearns Samuel. Adaptive signal processing. *Englewood Cliffs, NJ: Prentice Hall*, 1985.

[7] JM Ku, WB Jeong, and C Hong. Active control of compressor noise in the machinery room of refrigerators. *Noise Control Engineering Journal*, 67(5):350–362, 2019.

[8] Jeong-Mo Ku, Weui-Bong Jeong, and Chinsuk Hong. Controller design for active noise control of compressor by using the time window pocs technique. *Journal of Mechanical Science and Technology*, 34(7):2693–2700, 2020.

[9] Shiv Ram Meena and CS Rai. Effect of eigenvalue spread in noise cancellation of two sensory systems using adaptive algorithms. *Journal of Statistics and Management Systems*, 23(1):157–169, 2020.

[10] Reeves Fletcher and Colin M Reeves. Function minimization by conjugate gradients. *The computer journal*, 7(2):149–154, 1964.

[11] Giridhar K Boray and Mandyam D Srinath. Conjugate gradient techniques for adaptive filtering. In *1989 IEEE International Symposium on Circuits and Systems (ISCAS)*, pages 1752–1757. IEEE, 1989.

[12] Lu Lu, Guangya Zhu, Xiaomin Yang, and Kai Zhou. Conjugate gradient-based flann algorithms in nonlinear active noise control. *Journal of the Franklin Institute*, 359(9):4468–4488, 2022.

[13] John C Burgess. Active adaptive sound control in a duct: A computer simulation. *The Journal of the Acoustical Society of America*, 70(3):715–726, 1981.

[14] David G Luenberger and Ye Yinyu. *Linear and Nonlinear Programming*, volume 228. Springer International Publishing, fourth edition, 2015.

[15] Pi Sheng Chang and Alan N Willson. Analysis of conjugate gradient algorithms for adaptive filtering. *IEEE Transactions on Signal Processing*, 48(2):409–418, 2000.

[16] Jonathan Richard Shewchuk et al. An introduction to the conjugate gradient method without the agonizing pain, 1994.

[17] Lawrence E Kinsler, Austin R Frey, Alan B Coppens, and James V Sanders. *Fundamentals of acoustics*. John wiley & sons, 2000.

[18] Xu Wang. *Vehicle noise and vibration refinement*. Elsevier, 2010.

[19] Hans-Elias De Bree et al. The microflown: An acoustic particle velocity sensor. *Acoustics Australia*, 31(3):91–94, 2003.

[20] Kihong Shin and Joseph Hammond. *Fundamentals of signal processing for sound and vibration engineers*. John Wiley & Sons, 2008.